

GenFace: A Large-Scale Fine-Grained Face Forgery Benchmark and Cross Appearance-Edge Learning

Yaning Zhang, Zitong Yu, Xiaobin Huang, Linlin Shen, Jianfeng Ren

Abstract—The rapid advancement of photorealistic generators has reached a critical juncture where the discrepancy between authentic and manipulated images is increasingly indistinguishable. Thus, benchmarking and advancing techniques detecting digital manipulation become an urgent issue. Although there have been a number of publicly available face forgery datasets, the forgery faces are mostly generated using GAN-based synthesis technology, which does not involve the most recent technologies like diffusion. The diversity and quality of images generated by diffusion models have been significantly improved and thus a much more challenging face forgery dataset shall be used to evaluate SOTA forgery detection literature. In this paper, we propose a large-scale, diverse, and fine-grained high-fidelity dataset, namely GenFace, to facilitate the advancement of deepfake detection, which contains a large number of forgery faces generated by advanced generators such as the diffusion-based model and more detailed labels about the manipulation approaches and adopted generators. In addition to evaluating SOTA approaches on our benchmark, we design an innovative cross appearance-edge learning (CAEL) detector to capture multi-grained appearance and edge global representations, and detect discriminative and general forgery traces. Moreover, we devise an appearance-edge cross-attention (AECA) module to explore the various integrations across two domains. Extensive experiment results and visualizations show that our detection model outperforms the state of the arts on different settings like cross-generator, cross-forgery, and cross-dataset evaluations. Code and datasets will be available at <https://github.com/Jenine-321/GenFace>.

Index Terms—Face forgery benchmark, Transformer, Deepfake detection, Appearance-edge fusion

I. INTRODUCTION

Photorealistic synthesis technologies [9]–[11], especially the latest deep learning-based generative models such as gener-

This work was supported by National Natural Science Foundation of China No. 62306061. The work was also supported by open project of National Engineering Laboratory for Big Data System Computing Technology, Shenzhen University, Shenzhen 518060, PR China. (Yaning Zhang and Zitong Yu contributed equally to this work.) (Corresponding author: Linlin Shen)

Y. Zhang and X. Huang are affiliated with Computer Vision Institute, College of Computer Science and Software Engineering, Shenzhen University, Shenzhen, 518060, China. E-mail: zhangyaning0321@163.com and 2017192014@email.szu.edu.cn

Z. Yu is with School of Computing and Information Technology, Great Bay University, Dongguan, 523000, China, and also with National Engineering Laboratory for Big Data System Computing Technology, Shenzhen University, Shenzhen 518060, China. E-mail: yuzitong@gbu.edu.cn

L. Shen is with Computer Vision Institute, College of Computer Science and Software Engineering, Shenzhen University, Shenzhen, 518060, China, also with National Engineering Laboratory for Big Data System Computing Technology, Shenzhen University, Shenzhen, 518060, China, also with Shenzhen Institute of Artificial Intelligence and Robotics for Society, Shenzhen, 518129, China, and also with Guangdong Key Laboratory of Intelligent Information Processing, Shenzhen University, Shenzhen, 518060, China. E-mail: llshen@szu.edu.cn

J. Ren is with the School of Computer Science, University of Nottingham Ningbo China. E-mail: Jianfeng.Ren@nottingham.edu.cn

TABLE I: An overview of face forgery datasets. IQA: Image quality assessment. FG: Fine-grained; FF++: Faceforensics++; DFDC: Deepfake detection challenge; DF-1.0: Deepforensics; DFFD: Diverse fake face dataset.

Dataset	Generator			Public Availability	Real Images	Fake Images	Image Resolution	IQA Score	Year
	Diff.GAN	Attribute Editing	FG Label						
UADFV [1]	×	✓	×	✓	241	252	294×500	6.13	2019
FakeSpotter [2]	×	✓	✓	×	6,000	5,000	-	-	2019
FF++ [3]	×	✓	×	✓	-	-	480×1080	6.51	2019
Celeb-DF [4]	×	✓	×	✓	-	-	256×256	6.64	2020
DFDC [5]	×	✓	×	✓	-	-	256×256	6.62	2020
DF-1.0 [6]	×	✓	×	✓	-	-	1920×1080	6.93	2020
DFFD [7]	×	✓	✓	✓	58,703	240,336	299×299	6.95	2020
ForgeryNet [8]	×	✓	✓	✓	1,438,201	1,457,861	240×1080	6.15	2021
GenFace	✓	✓	✓	✓	100,000	515,000	256×1024	6.98	2024

ative adversarial network (GAN) [10], [12], [13] and denoising diffusion probabilistic models (DDPM) [14], have made remarkable progress in generating facial fake images, which leads to widespread public concerns about massive malicious abuse of them [15], [16]. Consequently, benchmarking and advancing facial forgery analysis has become a critical and urgent issue to benefit face forgery detection.

Face digital manipulation attacks, namely deepfake, generate forgery faces using deep learning-based methods, which mainly involve three categories, i.e., entire face synthesis (EFS) [12]–[14], attribute manipulation (AM) [17]–[19], and face swap (FS) [20], [21]. As Fig. 1 shows, EFS intends to yield non-existing fake faces from random noises with generative techniques. AM aims to edit facial attributes of an original image to produce a new forgery face with deep learning-based models. FS proposes to substitute the identity of source images with that of target images using neural networks. The above digital face forgery techniques facilitate the creation of deepfake datasets.

However, there are the following limitations for existing deepfake datasets: **(1) Small-scale forgery images:** As Table I shows, some early datasets such as UADFV [1] and FakeSpotter [2] contain fewer than 10,000 forgery images. **(2) Low image resolution and quality:** Existing efforts [1], [4], [5], [7] generate forgery images with resolutions smaller than 1024×1024. **(3) Coarse-grained labels:** Some recent works [3]–[7] only provide a coarse-grained manipulation label (real or fake). Fine-grained labels are rarely available. **(4) Poor diversity:** Most works [1], [3]–[8] tend to synthesize facial images through GAN-based generative networks such as StyleGAN [22], while novel generative techniques are hardly considered. To solve the above challenges, inspired by [23], we construct a large-scale, hierarchical, and fine-grained high-fidelity deepfake dataset, namely GenFace, which introduces

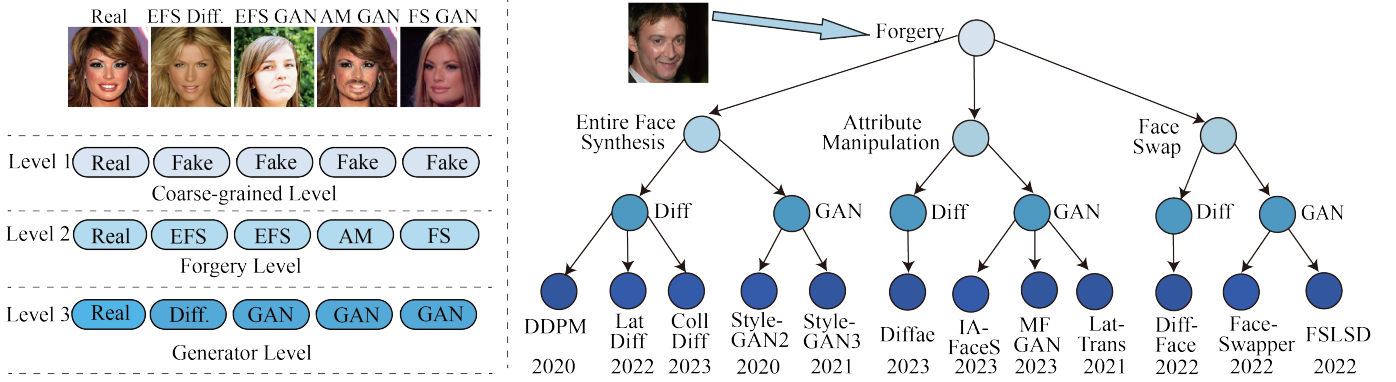


Fig. 1: Taxonomy of the GenFace dataset. At level 1, we divide images into real or fake faces. The second level, i.e., forgery level, classifies forged images into three types, i.e., entire face synthesis (EFS), attribute manipulation (AM), and face swap (FS). Then, we separate images based on whether forgery approaches are diffusion-based or GAN-based. The final level refers to the specific generators. LatDiff is LatentDiffusion. CollDiff is CollaborativeDiffusion. MF GAN is MaskFace GAN. LatTrans is LatentTransformer.

face forgery images generated by diffusion-based models to provide fine-grained forgery labels. Unlike [23] which is applied to image manipulation detection in general natural scenes, our dataset is designed for face forgery detection. Specifically, as displayed in Fig. 1, we divide deepfakes into three types, i.e., EFS, AM, and FS. We then categorize EFS into diffusion-based and GAN-based methods. AM and FS are both divided into GAN-based approaches. Each category contains some specific generators, and we provide sample labels at each level. In detail, we generate entire fake face images using StyleGAN2 [13], StyleGAN3 [12], and DDPM [14], since StyleGAN2 redesigns the normalization layer, and introduces progressive training techniques to gradually increase image resolution, yielding clearer and more detailed images than StyleGAN. However, a large variety of image details created by StyleGAN2 appear to be fixed in pixel coordinates, leading to the texture sticking issue. To solve this problem, StyleGAN3 [12] designs the rotation equivariance formula to achieve translation and rotation invariance, which significantly improves the quality of synthesized images. DDPM [14] models the conditional probability distribution of pixels, and introduces deformation operations and multi-scale modeling, thereby generating images with better diversity, richness, and realism.

Large and diverse high-quality deepfake datasets also promote the development of face forgery detection networks. Most detectors [24]–[26] treat deepfake detection as a binary classification problem, examining manipulated artifacts to discern authenticity using neural networks. To capture comprehensive forgery patterns, some works [24], [25] leverage hybrid transformer-based networks to capture local and global appearance representations. However, (1) they are not good at capturing high-frequency information in the appearance domain [27]. (2) They capture local or global forgery traces only in the appearance domain, limiting their representation ability. In this work, we aim to introduce discriminative features as complementary information, to facilitate deepfake

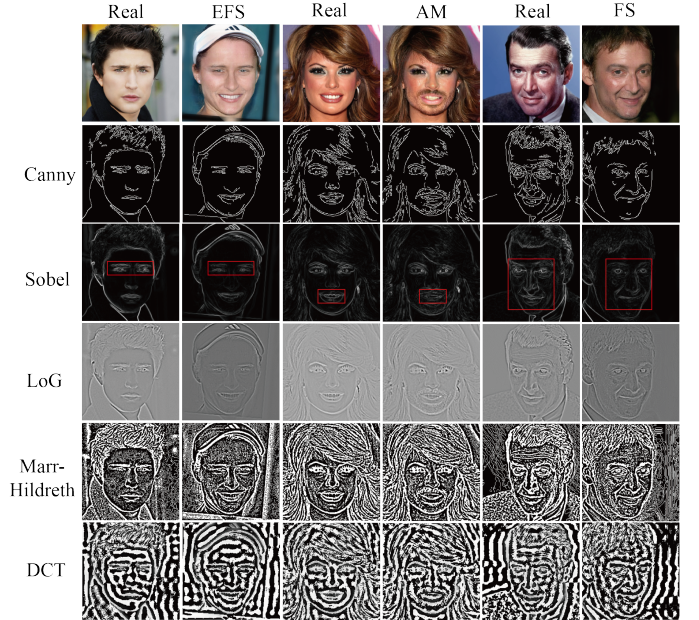


Fig. 2: The visualization of images produced by different operators. The first row represents the RGB images. Every two columns display the real and fake samples of various manipulations.

detection. We are motivated by the observation that there are significant differences between authentic and forgery edge images extracted by Sobel [28] (see Fig. 2), compared to other operators such as edge Canny [29], Laplacian of Gaussian (LoG) [30], and MarrHildreth [31], as well as the frequency-based discrete cosine transform (DCT) [32]. Therefore, we utilize the Sobel operator to obtain edge images, and design the edge transformer encoder to explore global forgery traces in the edge domain. Furthermore, inspired by [25], we design a fine-grained transformer encoder to extract fine-grained appearance global manipulated features. A coarse-

grained transformer encoder is proposed to explore coarse-grained global forgery artifacts, to retain high-frequency details in the appearance domain. Moreover, a multi-grained cross-attention module is introduced to explore diverse and comprehensive forgery patterns by integrating multi-grained appearance global embeddings, since counterfeit patterns exist and vary at different image granularities [33]. To achieve better interactions between the appearance and edge domains, we devise an appearance-edge cross-attention (AECA) module to mine complementary and diverse forgery traces. In summary, the contributions of our work are as follows:

- To the best of our knowledge, we conduct the first non-video, diverse, large-scale, and fine-grained deepfake image dataset, namely GenFace, to facilitate deepfake detection, which contains face forgery images generated by state-of-the-art synthesis techniques like diffusion, and eliminates the need for volunteers to participate in face swap, considerably reducing the cost of data collection.
- We design a novel cross appearance-edge learning (CAEL) detector, which captures multi-grained appearance and edge global forgery patterns, and explores the diverse fusion across two domains to mine complementary and comprehensive forgery artifacts.
- We conduct a comprehensive benchmarking evaluation using GenFace, demonstrating the effectiveness of the proposed CAEL through cross-generator, cross-forgery, and cross-dataset evaluation.

II. RELATED WORKS

Deepfake datasets. Comprehensive and extensive benchmarks for deepfake detection are limited in the community. Wang et al. [2] created a dataset with entire fake face images generated by the pre-trained ProGAN [34] and StyleGAN2 [13]. To further increase the diversity of the benchmark, DFFD [7] created the deepfake dataset with facial attribute edited images using Face APP, and entire fake face images produced by StarGAN. Video-based face forgery models became available with the release of FaceForensics [35], which contains Face2Face [36] manipulated frames from over 1,000 videos. An enhanced version, FaceForensics++ (FF++) [37], expands the collection to include Deepfake [38] and FaceSwap [39] manipulations. However, the above datasets are limited to GAN-based methods such as StyleGAN. For each manipulation type, they hardly take the fine-grained partitioning such as diffusion-based or GAN-based, into account. To address this limitation, we construct the first large-scale, hierarchical, and fine-grained deepfake dataset with diverse and most recent forgery methods, including entire fake face images using DDPM [14], LatentDiffusion [40], Collaborative Diffusion [41], StyleGAN2 [13], and StyleGAN3 [12], face attribute manipulated images using LatentTransformer [17], MaskFaceGAN [19], Diffae [42] and IAFaceS [18], and face-swapped images generated by FaceSwapper [20], DiffFace [43] and FSLSD [21].

Deepfake detection. Existing deep learning-based models have been proposed to detect the security threat caused by deepfake forensics. Dang et al. [7] leveraged the Xception

TABLE II: The outline of generator details. Image source means the original dataset that generators are trained on. CollDiffusion means collaborative diffusion.

Forgery Method	Forgery Type	Image Source	Image Number	Image Resolution	Year
DDPM [14]	EFS	CelebAHQ	50k	256×256	2020
LatentDiffusion [40]	EFS	CelebAHQ/FFHQ	60k	256×256	2022
CollDiffusion [41]	EFS	CelebAHQ	50k	512×512	2023
StyleGAN2 [13]	EFS	FFHQ	50k	1024×1024	2020
StyleGAN3 [12]	EFS	CelebAHQ	50k	256×256	2021
FaceSwapper [20]	FS	CelebA	30k	256×256	2022
DiffFace [43]	FS	CelebAHQ	30k	1024×1024	2022
FSLSD [21]	FS	CelebAHQ	30k	1024×1024	2022
LatentTransformer [17]	AM	CelebAHQ	60k	1024×1024	2021
Diffae [42]	AM	FFHQ	70k	256×256	2023
IAFaceS [18]	AM	CelebAHQ	5k	256×256	2023
MaskFaceGAN [19]	AM	CelebAHQ	30k	1024×1024	2023

backbone to capture local forgery patterns for deepfake detection, which rarely considers global information. To address this problem, Wodajo et al. [24] designed a convolutional vision transformer (CViT) that combines CNN with the vision transformer (ViT) to identify authenticity. Coccomini et al. [25] studied global forgery traces by integrating EfficientNet with ViT. To further explore comprehensive forgery patterns, they also encoded multi-scale global features by combining EfficientNet with a cross-attention multi-scale vision transformer (CrossViT) for deepfake detection. To enrich embeddings, a multi-modal multi-scale transformer (M2TR) [33] model attempts to introduce high-frequency features extracted by DCT, and fuse them with multi-scale embeddings. Spatial-frequency dynamic graph (SFDG) [44] exploits the relation-aware features in spatial and frequency domains via dynamic graph learning. GramNet [45] leverages global image texture representations for robust fake image detection. Diffusion reconstruction error (DIRE) [46] measures the error between an input image and its reconstruction counterpart by a pre-trained diffusion model to distinguish between the real and fake images. Universalfakedetect (UFD) [47] utilizes a feature space not explicitly trained to discern authenticity via nearest neighbor and linear probing as instantiations. By contrast, our method is capable of examining global edge forgery traces, as well as multi-grained appearance-edge fusion representations.

III. GENFACE CONSTRUCTION

A. Data Collection

Original real images. CelebAHQ [34] is selected as the original real image dataset, which consists of 30,000 images with a resolution of 1024 × 1024, and is a high-quality version of the CelebA dataset. CelebA [48] includes 10,000 identities, each of which has a collection of twenty images, making a total of 200,000 images. These images are subjected to a series of high-quality processing and image quality assessments, sorted accordingly, and the top 30,000 high-resolution 1024 × 1024 images are retained as the CelebAHQ dataset. We also choose the flickr-faces-HQ (FFHQ) [49] dataset as the original real image dataset, which is a high-quality face image dataset consisting of 70,000 high-quality images at 1024×1024

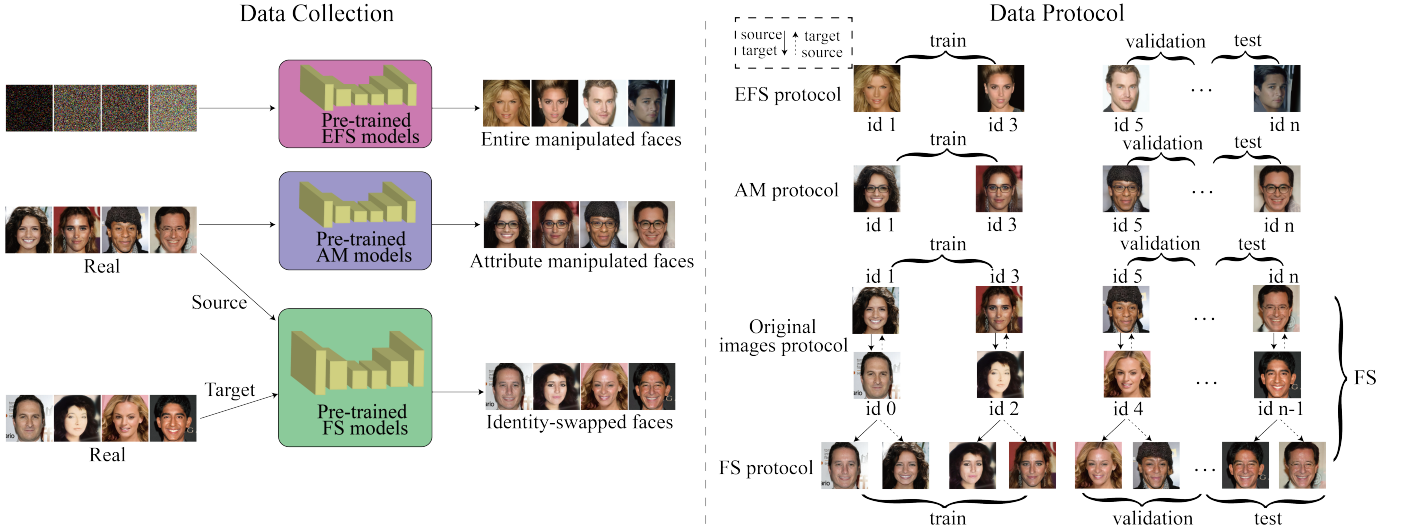


Fig. 3: Schematic illustration of the collection and partitioning of GenFace.

resolution, containing considerable variation in age, ethnicity, and image background.

Entire face synthesis. As Fig. 3 shows, we input random noises into pre-trained diffusion-based or GAN-based models to synthesize fake faces. As Table II shows, for diffusion-based methods, we use CelebAHQ pre-trained DDPM [14] and LatentDiffusion [40], with a sampling step size of 100 and 50 to generate 50,000 and 30,000 images, respectively. The collaborative diffusion [41] pre-trained by CelebAHQ or FFHQ produces 30,000 images, respectively, with a sampling step of 100. For GAN-based methods, we leverage StyleGAN2 [13] pre-trained by FFHQ, and StyleGAN3 [12] pre-trained by CelebAHQ, to obtain 50,000 images each.

Attribute manipulation. We use facial attribute editing models [17]–[19] pre-trained by CelebAHQ to perform attribute manipulations on the original real faces. Since the model was trained using data from the same domain, the quality of the synthesized faces is higher. LatentTransformer [17] can edit forty types of facial attributes, including eyeglasses, bangs, bags, etc. We select some common categories such as eyeglasses and bushy eyebrows. We fed the original real images into LatentTransformer to generate 30,000 manipulated images for each attribute, respectively. MaskFaceGAN [19] can manipulate fourteen local attributes, and we chose the attribute of the big nose to produce 30,000 fake faces. We utilize IAFaceS [18] to manipulate five face attributes of real images, i.e., bags, beard, bushy, open mouth, and narrow eyes, to create 1,000 images for each attribute. For the diffusion-based model, the FFHQ pre-trained Diffae [42] is leveraged to create 70,000 attribute manipulated images.

Face swap. We leverage the pre-trained face swap model [20], [21] to synthesize fake faces from the source and target image. Specifically, as Fig. 3 shows, we divide the 30,000 original images into two groups, each of which has 15,000 images. One group serves as the source image, and the other group is used as the target object, forming 15,000 source and target image pairs. The identities of image pairs are exchanged to form 15,000 new source and target pairs. Each pair is passed through

the face swap model to produce identity-swapped face images. We employ FaceSwapper [20] pretrained on CelebA and FSLSD [21] pretrained on CelebAHQ, to generate 30,000 fake images each. For diffusion-based methods, we use CelebAHQ pre-trained DiffFace [43], with a sampling step size of 1000, to yield 30,000 face-swapped images, respectively.

B. Data Protocol

Original real images. CelebA is officially divided into three parts, i.e., 160,000 images of the first 8,000 identities for training, 20,000 images of another 1,000 identities for validation, and 20,000 images of the remaining 1,000 identities for testing. Since identities in CelebAHQ correspond to those in CelebA, we use CelebAHQ along with the official protocols, i.e., 24,183 images for training, 2,993 images for validation, and 2,824 images for testing, to ensure identity independence and exclusivity across all subsets. Similarly, FFHQ is officially split into two parts, i.e., 60,000 images for training, and 10,000 images for testing.

Entire face synthesis. Note that images from EFS are identity-independent. Therefore, 30,000 samples are selected for each generator of EFS to balance the two categories. We split them in the same ratio as the original image dataset, with 24,183 images in the training set, 2,993 images in the validation set, and 2,824 images in test set.

Attribute manipulation. We find that face attribute edited images are matched to the real images in terms of identity. Consequently, we adhere to the official partitioning for each generator, to ensure that the quantity and identity within each subset align with those in the real image dataset.

Face swap. As Fig. 3 illustrates, the identities of face-swapping images correspond to that of the source images from the CelebAHQ dataset. Therefore, for each generator, we adopt the official protocols to guarantee that the quantity and identity within each subset match those in the real image dataset.

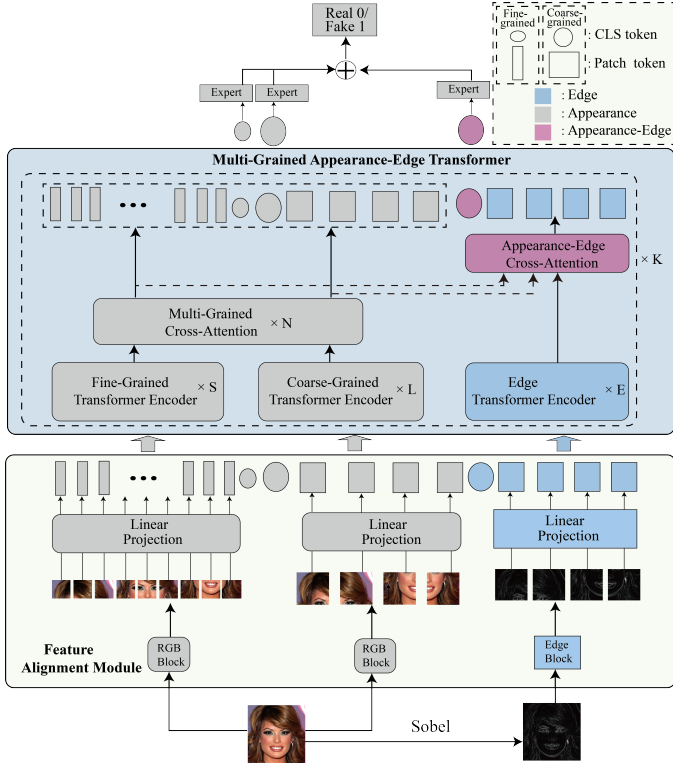


Fig. 4: The architecture of the proposed model. We first encode fine-grained appearance features, coarse-grained appearance representations, and edge embeddings from input RGB images and edge images via a feature alignment module, respectively. We then fed them into the multi-grained appearance-edge transformer (MAET) module to capture diverse appearance-edge forgery patterns, global edge features, and diverse mixture representations across two domains. Finally, they are sent to respective experts, and the integration of multiple experts yields the final prediction.

IV. DEEPPAKE DETECTION NETWORKS

To capture multi-grained appearance and edge forgery traces, we design cross appearance-edge learning (CAEL) for deepfake detection. As Fig. 4 shows, CAEL extracts appearance and edge embeddings, respectively, through the feature alignment module (see Sect. IV-A). After that, they are fed into the multi-grained appearance-edge transformer (MAET) module (see Sect. IV-B) to capture multi-grained appearance forgery patterns as well as global edge representations, and various synergies across two domains are explored through the AECA module (see Sect. IV-C). Finally, they are fed into respective experts consisting of fully connected layers, and the integration of multiple experts yields the final prediction.

A. Feature Alignment Module

Given an input face appearance image $X^a \in \mathbb{R}^{3 \times H \times W}$, where H and W denote the height and width, respectively, we utilize the Sobel operator to get the edge image $X^e \in \mathbb{R}^{1 \times H \times W}$. To align features in the embedding space, Fig. 4 shows that we send the X^a to two stream RGB blocks

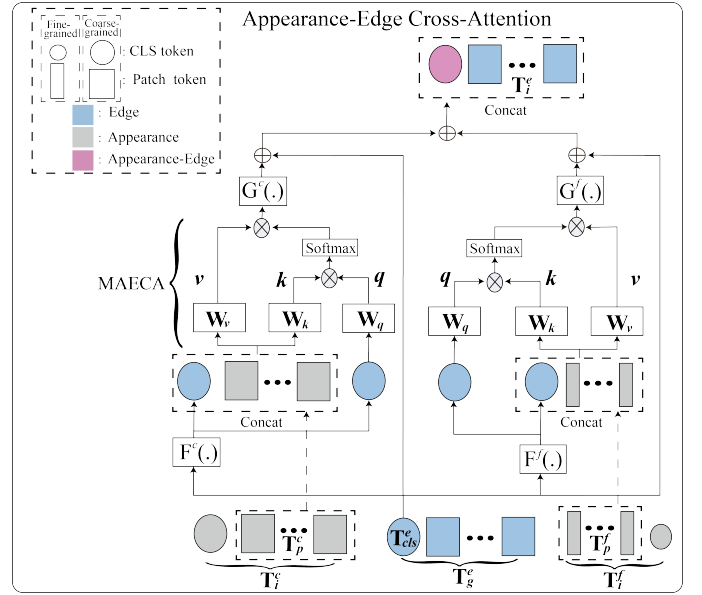


Fig. 5: The workflow of appearance-edge cross-attention.

with stacked convolutional layers to get the fine-grained features $X^f \in \mathbb{R}^{C \times (\frac{H}{32}) \times (\frac{W}{32})}$ and coarse-grained representations $X^c \in \mathbb{R}^{C \times (\frac{H}{4}) \times (\frac{W}{4})}$, respectively, where C denotes channels. Meanwhile, the edge image is fed into the edge block with stacked convolutional layers to yield edge local embeddings $X_l^e \in \mathbb{R}^{C \times (\frac{H}{4}) \times (\frac{W}{4})}$. To facilitate the extraction of global edge forgery traces, the feature patches in X_l^e are flattened as feature tokens along the channel, and then projected and attached to the class token, to get edge token representations $X_t^e \in \mathbb{R}^{(n+1) \times 2d}$, where n and d denote the number and dimension of the feature token, respectively. We can gain fine-grained and coarse-grained appearance token embeddings $X_t^f \in \mathbb{R}^{(n+1) \times d}$ and $X_t^c \in \mathbb{R}^{(n+1) \times 2d}$ in the same way, respectively. They are then added with the positional information, and transferred to the first transformer block in the MAET module.

B. Multi-Grained Appearance-Edge Transformer

Unlike traditional transformers [24], [25] that solely focus on local and global appearance information or multi-grained appearance global forgery patterns, we design the MAET module to encode edge global features and multi-grained appearance global embeddings, and comprehensively integrate them through the AECA module.

Specifically, as shown in Fig. 4, MAET mainly contains K transformer blocks, each of which is composed of a fine-grained transformer encoder with S blocks, a coarse-grained transformer encoder with L blocks, an edge transformer encoder with E blocks, a multi-grained cross-attention module with N blocks and an AECA module. The first three transformer encoders adopt the same architecture as ViT. Inspired by [25], the multi-grained cross-attention module is introduced to mine the multi-grained fused forgery traces.

In detail, given fine-grained appearance tokens $T^f \in \mathbb{R}^{(n+1) \times d}$, coarse-grained appearance tokens $T^c \in \mathbb{R}^{(n+1) \times 2d}$, and edge tokens $T^e \in \mathbb{R}^{(n+1) \times 2d}$, we send them to the

fine-grained transformer encoder, coarse-grained transformer encoder, and edge transformer encoder to obtain global forgery patterns $T_g^f \in \mathbb{R}^{(n+1) \times d}$, $T_g^c \in \mathbb{R}^{(n+1) \times 2d}$, and $T_g^e \in \mathbb{R}^{(n+1) \times 2d}$, respectively. To flexibly fuse multi-grained appearance representations, T_g^f and T_g^c are then fed into the multi-grained cross-attention module to obtain integrated global forgery traces at different granularities $T_i^f \in \mathbb{R}^{(n+1) \times d}$ and $T_i^c \in \mathbb{R}^{(n+1) \times 2d}$. The detailed workflow of the module is discussed in this work [50]. To facilitate diverse global interactions between edge and multi-grained appearance features, we design the AECA module to produce $T_i^e \in \mathbb{R}^{(n+1) \times 2d}$ by inputting T_i^f , T_i^c , and T_g^e . That is:

The detailed workflow of AECA is discussed in Section IV-C. After that, we transfer T_i^f , T_i^c , and T_i^e into the subsequent transformer block.

C. Appearance-Edge Cross-Attention

To fuse the multi-grained appearance-edge representations more efficiently and effectively, we first employ the edge class token as a query to swap information among the fine-grained and coarse-grained appearance patch tokens, respectively, and then back project it to its own branch. Since the edge class token already captures the edge information among all its own patch tokens, interacting with the appearance patch tokens from various granularity helps to fuse appearance and edge information, comprehensively. After the integration across two domains, the edge class token interacts with its own patch tokens again at the next transformer block, where it passes the learned knowledge from different grained appearance tokens to its own edge patch token, to enrich the embedding of each patch token. In detail, as Fig. 5 illustrates, given fine-grained appearance tokens $T_i^f \in \mathbb{R}^{(n+1) \times d}$, coarse-grained appearance tokens $T_i^c \in \mathbb{R}^{(n+1) \times 2d}$, and edge tokens $T_g^e \in \mathbb{R}^{(n+1) \times 2d}$, we can obtain the edge class token $T_{cls}^e \in \mathbb{R}^{1 \times 2d}$, fine-grained appearance patch tokens $T_p^f \in \mathbb{R}^{n \times d}$, and coarse-grained appearance patch tokens $T_p^c \in \mathbb{R}^{n \times 2d}$. The T_{cls}^e serves as a query to interact with T_p^f and T_p^c , respectively. The workflow of the fusion between T_{cls}^e and T_p^f is as follows:

Firstly, to boost the information exchange, we project T_{cls}^e to obtain $T_{cls}^{ef} \in \mathbb{R}^{1 \times d}$, i.e., $T_{cls}^{ef} = F^f(T_{cls}^e)$, and concatenate it with T_p^f to get $T_{all}^{ef} \in \mathbb{R}^{(n+1) \times d}$, where F^f is the projection function for dimension alignment. We then conduct multi-head appearance-edge cross-attention (MAECA) between T_{cls}^{ef} and T_{all}^{ef} . Mathematically, the calculation of MAECA is as follows:

Then, the appearance-edge cross-attention weights are calculated as follows:

$$A = \text{softmax}\left(\frac{qk^T}{\sqrt{d_m}}\right), \quad (1)$$

where $A \in \mathbb{R}^{1 \times (n+1)}$ denotes the attention map between appearance and edge tokens. Note that we only use the class token as a query, the computational cost of producing the attention map in A is linear instead of quadratic like vanilla MHSA, which makes the entire process more efficient.

After that, to achieve global fusion between edge and fine-grained appearance representations, we design the formula as below:

$$\text{MAECA}(T_{all}^{ef}) = Av. \quad (2)$$

TABLE III: Cross-generator evaluation. ACC and AUC scores (%) of different approaches trained and tested using images produced by diffusion and GAN generators. The best results are in bold.

Training Set	Model	Testing Set			
		Diffusion-syn.		GAN-syn.	
		ACC	AUC	ACC	AUC
Diffusion-syn.	ResNet [51]	100	100	50.02	73.92
	Xception [26]	100	100	50.00	58.29
	VGG [52]	100	100	50.00	57.85
	ViT [53]	99.19	99.96	49.88	49.46
	CrossViT [50]	99.50	99.98	50.14	54.32
	iFormer [27]	100	100	50.00	43.72
	CViT [24]	100	100	50.00	60.20
	EViT [25]	99.89	100	50.02	61.66
	CEViT [25]	99.98	100	50.50	86.45
	SFDG [44]	99.95	100	50.08	62.74
	GFF [54]	99.98	100	50.15	63.21
	GramNet [45]	99.95	100	50.23	70.15
	DIRE [46]	99.99	100	50.57	87.12
	UFD [47]	99.95	100	50.34	87.35
	Ours	100	100	50.60	92.73
GAN-syn.	ResNet [51]	49.99	54.45	99.79	99.99
	Xception [26]	49.99	54.45	99.79	99.99
	VGG [52]	49.81	61.61	99.66	99.99
	ViT [53]	49.62	39.06	98.67	99.92
	CrossViT [50]	49.92	44.29	98.69	99.88
	iFormer [27]	49.82	45.21	99.82	100
	CViT [24]	50.03	50.29	99.81	99.98
	EViT [25]	49.87	43.94	100	100
	CEViT [25]	50.09	75.89	100	99.88
	SFDG [44]	50.07	52.35	100	99.96
	GFF [54]	50.09	53.12	100	99.98
	GramNet [45]	50.12	75.29	100	100
	DIRE [46]	50.08	74.78	100	100
	UFD [47]	50.10	75.68	100	99.97
	Ours	50.13	83.02	100	100

Thereafter, the output of MAECA is projected and added to T_{cls}^e to get $T_{cls}^{ef} \in \mathbb{R}^{1 \times 2d}$. The interaction between T_{cls}^e and T_p^c follows the same workflow as that between T_{cls}^e and T_p^f . Therefore, we can obtain $T_{cls}^{ec} \in \mathbb{R}^{1 \times 2d}$ with the fused edge and coarse-grained appearance forgery patterns. Finally, we enhance the communication between T_{cls}^{ef} and T_{cls}^{ec} , and then concatenate it with the edge patch tokens T_p^e , which can be formulated as:

$$T_i^e = [(T_{cls}^{ef} + T_{cls}^{ec}) || T_p^e]. \quad (3)$$

V. EXPERIMENTS

A. Implementation Details

We developed the detector using PyTorch on the Tesla V100 GPU with batch size 32. The number of blocks K , S , L , E , and N in CAEL is set to 4, 2, 3, 3, and 2, respectively. The attention heads m are set to 8 and the dimension of the feature token d is set to 192. We employed the argumentations library [55] for data augmentation. Our model is trained with the Adam optimizer [56] with a learning rate of 1e-4 and weight decay of 1e-4. We utilized the scheduler to drop the

TABLE IV: Cross-generator evaluation. ACC and AUC scores (%) on each facial attribute edited by IAFaceS, after training using images manipulated by LatentTransformer.

Model	Attribute Manipulation										Average
	bags		beard		bushy		open mouth		narrow eyes		
	ACC	AUC	ACC	AUC	ACC	AUC	ACC	AUC	ACC	AUC	
ResNet [51]	50.00	49.31	50.00	60.30	50.00	50.07	50.00	52.79	50.00	53.24	53.14
Xception [26]	49.95	47.88	50.10	40.13	50.00	52.15	49.95	49.64	50.00	52.22	48.40
VGG [52]	49.95	48.18	49.95	46.22	49.95	49.88	49.95	50.62	50.00	64.69	51.92
ViT [53]	49.90	44.93	49.85	45.40	49.80	50.72	49.85	51.12	50.50	47.60	47.95
CrossViT [50]	50.05	46.93	50.00	48.75	49.95	50.77	49.85	49.36	50.10	45.58	48.28
iFormer [27]	50.00	54.14	50.00	53.28	50.00	53.89	50.00	55.70	50.00	56.20	54.64
CViT [24]	50.05	50.88	50.00	44.63	50.05	50.37	50.00	51.27	50.00	49.58	49.35
EViT [25]	50.00	53.62	50.05	51.55	50.00	55.19	50.00	54.10	50.00	54.96	53.88
CEViT [25]	50.00	55.57	50.00	49.31	50.00	57.61	50.05	56.23	50.00	55.32	54.81
SFDG [44]	50.00	54.65	50.01	50.54	50.00	55.61	50.03	54.23	50.09	54.32	55.87
GFF [54]	50.00	60.14	50.00	50.65	50.02	57.14	50.02	56.17	50.03	55.62	57.81
GramNet [45]	50.01	60.73	50.02	59.31	50.05	57.52	50.04	59.03	50.13	60.21	63.65
DIRE [46]	50.04	61.07	50.03	60.15	50.04	59.41	50.03	60.74	50.34	61.32	63.47
UFD [47]	50.02	60.41	50.01	60.36	50.04	60.41	50.03	60.21	50.15	60.25	64.36
Ours	50.00	69.84	50.00	77.35	50.10	73.43	50.05	71.09	50.00	71.62	72.67

learning rate by ten times every 15 epochs. We leveraged the cross-entropy loss function to train our model.

Evaluation Metrics. We employed accuracy (ACC) and area under the receiver operating characteristic curve (AUC) as our evaluation metrics.

B. GenFace Benchmark

We conducted the within-dataset evaluation including cross-forgery evaluation and cross-generator evaluation, cross-dataset evaluation, fine-grained classification, and facial image frequency analysis on GenFace.

We evaluated state-of-the-art deepfake detection approaches on our benchmark dataset. We selected common CNN-based models such as ResNet-18 [51], VGG-16 [52], Xception [26], general transformer-based approaches including ViT-B [53], CrossViT-B [50], and iFormer-B [27] and some detectors such as UFD [47] and DIRE [46] which are specifically designed to detect diffusion-generated images. We also selected some hybrid transformer-based deepfake detectors such as CViT [24], EViT [25], and CEViT [25] as well as the recent SOTA detectors including SFDG [44], GFF [54], and GramNet [45].

Cross-forgery evaluation. To evaluate our dataset, we conducted cross-forgery tests. We trained models using images of one manipulation, and tested them on those of each manipulation, i.e., EFS, AM, and FS, respectively. The results are displayed in Table V. We can observe that most models achieve poor performance (about 70% AUC) on cross-forgery evaluation, which justifies the high image quality of our challenging GenFace dataset. For transformer-based detectors, the AUC of our network is around 21.6%, 25.1%, and 2.3% higher than that of CViT, EViT, and CEViT, respectively, on FS after training using AM, which is attributed to the powerful fusion capabilities across multi-grained appearance and edge information.

Cross-generator evaluation. To perform fine-grained analysis, we examined the performance of detectors on cross-generator evaluation. We trained models using images of one generator from EFS, and tested them on different generators,

TABLE V: Cross-forgery generalization. ACC and AUC scores (%) on each manipulation, after training using one manipulation.

Training Set	Model	Testing Set					
		EFS		AM		FS	
		ACC	AUC	ACC	AUC	ACC	AUC
EFS	ResNet [51]	100	100	50.00	46.86	74.98	70.75
	Xception [26]	100	100	50.00	63.14	68.06	79.52
	VGG [52]	100	100	50.00	67.02	75.00	75.27
	ViT [53]	95.31	99.81	54.69	65.86	53.13	61.43
	CrossViT [50]	98.46	99.93	49.89	53.65	69.23	74.53
	iFormer [27]	100	100	50.00	62.66	74.96	73.21
	CViT [24]	99.98	100	50.02	63.53	72.79	73.82
	EViT [25]	99.36	100	50.03	70.58	74.61	78.58
	CEViT [25]	99.99	100	50.00	75.41	74.95	78.32
	SFDG [44]	99.64	100	50.02	73.54	73.82	75.93
	GFF [54]	99.52	100	50.01	74.32	73.91	76.43
	GramNet [45]	99.61	100	50.05	76.24	74.21	76.13
	DIRE [46]	99.94	100	50.03	76.14	74.03	77.89
	UFD [47]	99.98	100	50.04	76.32	74.76	78.01
	Ours	100	100	50.04	83.31	75.00	79.96
AM	ResNet [51]	50.17	71.06	99.98	100	49.98	69.36
	Xception [26]	50.20	51.45	99.89	100	50.11	54.57
	VGG [52]	50.04	75.24	99.95	100	50.00	69.20
	ViT [53]	50.29	60.37	99.63	99.99	50.19	55.04
	CrossViT [50]	51.21	69.79	99.11	99.98	52.66	77.68
	iFormer [27]	50.20	72.38	99.98	100	50.42	78.27
	CViT [24]	50.15	70.32	99.89	100	50.02	60.74
	EViT [25]	50.26	56.65	99.91	100	49.95	57.28
	CEViT [25]	50.13	73.38	99.98	100	50.07	80.06
	SFDG [44]	50.15	60.73	99.93	100	50.03	59.37
	GFF [54]	51.02	62.75	99.96	100	50.08	59.21
	GramNet [45]	51.10	63.25	99.95	100	50.09	60.35
	DIRE [46]	51.14	72.41	99.94	100	51.24	70.45
	UFD [47]	50.65	73.40	98.65	100	52.36	71.89
	Ours	50.10	87.46	100	100	50.19	82.35
FS	ResNet [51]	50.24	73.13	50.41	76.85	99.88	100
	Xception [26]	50.42	76.48	53.75	75.62	99.84	99.99
	VGG [52]	50.22	72.37	49.98	79.66	99.98	100
	ViT [53]	51.09	69.16	52.37	78.11	99.19	99.97
	CrossViT [50]	50.59	62.06	50.69	66.02	98.85	99.94
	iFormer [27]	50.63	72.56	53.84	80.94	99.93	100
	CViT [24]	50.22	73.88	49.98	73.75	99.96	100
	EViT [25]	53.50	80.68	50.21	64.36	99.50	99.99
	CEViT [25]	53.64	80.96	50.45	73.84	99.97	100
	SFDG [44]	53.65	80.71	50.15	66.72	99.63	100
	GFF [54]	53.71	81.27	51.34	68.25	99.76	100
	GramNet [45]	54.83	80.89	51.19	67.13	99.74	100
	DIRE [46]	54.06	79.65	52.13	78.32	99.54	99.98
	UFD [47]	53.48	80.62	53.45	79.04	99.61	99.99
	Ours	56.65	88.41	50.99	78.32	99.98	100

i.e., diffusion-based and GAN-based generators, respectively. As Table III displays, models trained using diffusion-based generators outperform those trained with GAN-based methods. For instance, ResNet achieves 100% AUC and 73.92% AUC on the intra-generator and cross-generator testing, respectively, after training using images of the diffusion-based generator. By contrast, it only gains 99.99% AUC and 54.45% AUC when trained using the images of the GAN-based generator, which demonstrates that the diffusion-based generator tends to push models to study discriminative and comprehensive forgery artifacts, thus further enhancing detection accuracy. Models consistently achieve poorer performance on diffusion-

TABLE VI: Impacts of various operators. MH means Mar-Hildreth.

Training Set	Model	Testing Set	
		GAN-syn.	
		ACC	AUC
Diffusion-syn.	CAEL w/MH	50.46	84.69
	CAEL w/LoG	50.05	48.59
	CAEL w/DCT	50.33	90.21
	CAEL w/Canny	50.05	45.86
	CAEL w/Sobel	50.60	92.73

TABLE VII: Network ablation.

Model	ACC	AUC
F	50.02	84.33
C	50.12	86.09
E	50.15	87.64
F+C	50.21	87.45
F+E	50.37	88.86
C+E	50.45	90.32
F+C+E	50.60	92.73

based generators than those on GAN-based ones in Fig. 9, on cross-generator evaluation, showing that the diffusion-based generator produces higher-quality synthetic faces, making it more challenging for models to detect the forgery traces.

In order to further conduct the in-depth study of GenFace, we trained models using face images with attribute manipulated by LatentTransformer, and tested them on five attributes manipulated by the IAFaceS generator, i.e., bags, beard, bushy, open mouth, and narrow eyes. In Table IV, we noticed that the manipulated beard attribute is more difficult for detectors to identify, but the manipulation of two attributes such as narrow eyes and bushy are easier to detect.

To confirm the high quality of our dataset, we conducted the cross-dataset evaluation. We trained different deepfake detection approaches using the FF++ dataset and tested them on other datasets, i.e., GenFace, FF++, DFDC, Celeb-DF, and DF-1.0, respectively. The results are shown in Table VIII. We can see that models consistently show poorer performance on GenFace, compared to other datasets, demonstrating that our GenFace dataset is more challenging.

C. Ablation Study

In order to investigate the contribution of each module to learning capacity, we observed the performance on cross-generator setting. As shown in Table VII, F, C, and E mean the fine-grained branch, coarse-grained branch, and edge branch, respectively. The gains from introducing the edge branch (+4.5%) are evident, demonstrating that various edge representations provide valuable information to benefit deepfake detection. Especially, the AUC achieves the maximum after

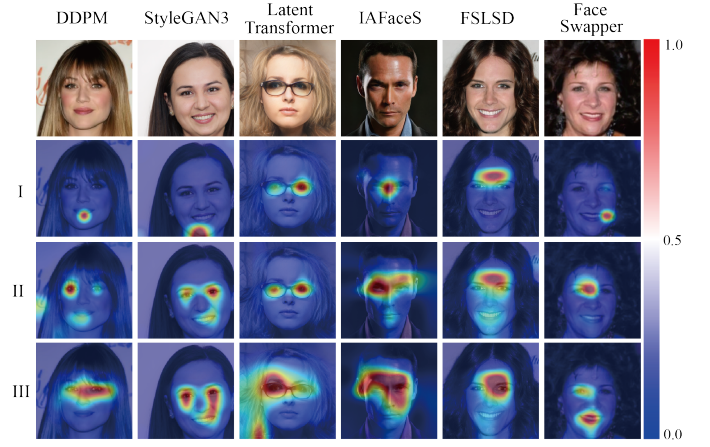


Fig. 6: The heatmap visualizations of various training settings on some examples from GenFace.

TABLE VIII: Cross-dataset evaluation. ACC and AUC scores (%) of different methods on GenFace, FF++, DFDC, Celeb-DF, and DF-1.0, after training on FF++.

Training Set	Model	Testing Set									
		GenFace		FF++		DFDC		Celeb-DF		DF-1.0	
		ACC	AUC	ACC	AUC	ACC	AUC	ACC	AUC	ACC	AUC
FF++	Xception [26]	53.85	60.61	90.49	96.72	60.27	66.95	54.24	65.86	59.40	63.59
	ResNet [51]	50.86	62.27	79.06	87.85	67.81	68.07	59.31	62.35	55.33	62.31
	CrossViT [50]	51.10	58.21	62.49	67.50	54.05	58.46	63.50	59.72	49.55	59.30
	CViT [24]	56.99	61.96	90.25	96.27	51.04	63.98	60.61	64.96	62.15	64.53
	SFDG [44]	53.74	59.13	90.30	96.71	60.24	67.31	55.29	63.48	58.21	61.48
	GFF [54]	54.61	60.27	91.08	97.64	61.15	68.02	57.12	62.37	60.14	62.74
	GramNet [45]	54.72	61.38	90.45	96.85	60.37	68.14	56.24	62.67	59.38	63.82
	DIRE [46]	55.74	61.25	90.86	97.85	62.45	66.74	59.75	60.12	60.41	63.87
	UFD [47]	56.21	61.89	90.69	97.03	62.26	67.03	59.96	61.35	60.56	63.98
	Ours	58.55	65.04	92.87	98.11	64.64	68.98	60.23	66.48	58.85	65.23

integrating multi-grained appearance embeddings with edge features.

D. Visualization and Discussion

We evaluated our detector by visualization, ablation study, and robustness analysis. We investigated the effect of different operators, various queries, different fusion schemes, appearance-edge cross-attention, the depth of the edge transformer encoder, and the number of multi-grained appearance-edge transformer blocks, respectively.

Visualization. To further investigate the effectiveness of our detector, In Fig. 6, we displayed the class activation mapping (CAM) of the sample, generated by each generator for three networks. Each column shows a forgery face yielded by various generative methods, including DDPM, StyleGAN3, LatentTransformer, etc. The second to fourth rows illustrate heatmaps for three models listed in Table V: (I) the EViT model; (II) CEViT; and (III) our CAEL network. CEViT (II) detects more long-range forgery patterns than EViT (I), which demonstrates the effectiveness of the fusion across multi-grained appearance features. In comparison to (II), CAEL (III) further captures more manipulated areas, showing that comprehensively integrating the edge information with multi-grained appearance embeddings can benefit deepfake detection.

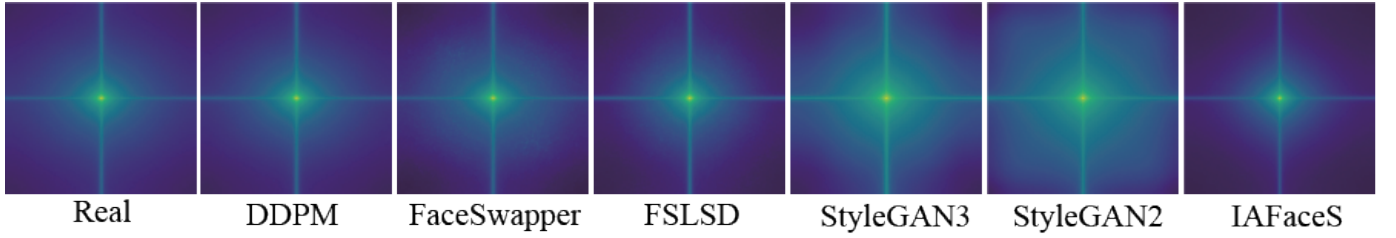


Fig. 7: The frequency visualization of facial images generated by various generators.

TABLE IX: Effects of various queries.

Training Set	Model	Testing Set			
		GAN-syn.			
		ACC	AUC	Params(M)	Flops(G)
Diffusion-syn.	Query w/cls	50.60	92.73	158.63	2.11
	Query w/patch	50.56	92.61	158.63	2.11
	Query w/all	50.58	92.64	158.63	2.12

TABLE X: The classification performance of the coarse-grained level.

Model	Coarse-grained Level	
	ACC	AUC
ResNet [51]	99.23	99.98
ViT [53]	96.32	96.94
CViT [24]	99.86	99.99
CEViT [25]	99.87	99.99
Ours	99.88	100

Impacts of different operators. We investigated the effect of various operators, including edge Sobel, Canny, LoG, and MarrHildreth, as well as the frequency-based DCT. We tested models on cross-generator setting. The results of ablation are shown in Table VI. When Sobel edge is involved, the AUC achieves the maximum. We believe that edge features extracted by Sobel are discriminative, which can further improve the detection performance.

Influence of various queries. For the AECA module of our method, we used the edge class token as the query. Next, we varied the query to see the effect on performance and efficiency. In Table IX, we noticed that the computational complexity of the model is increased by 0.01G, when all tokens are encompassed. Since the computational cost of creating an attention map is linear when the class token is used as a query, rather than quadratic like when all tokens serve as a query, this makes the whole process more efficient.

Classification performance of various levels. For coarse-grained detection, the experimental results are shown in Table X. The forgery level and generator level detection results of various models are displayed in Table XI and Table XII, respectively. ACC scores indicate that the classification becomes easier with the number of categories growing from 2 (coarse-grained level) to 4 (forgery level) and 5 (generator level). Moreover, our model consistently shows excellent performance on various level classifications, compared to other

TABLE XI: The classification performance of the forgery level.

Model	Forgery Level			
	ACC	Precision	Recall	F1
ResNet [51]	99.78	99.78	99.77	99.77
Xception [26]	99.66	99.66	99.66	99.66
ViT [53]	97.50	97.61	97.50	97.51
CViT [24]	99.83	99.83	99.83	99.82
CEViT [25]	99.88	99.88	99.88	99.87
Ours	99.95	99.95	99.95	99.95

TABLE XII: The classification performance of the generator level.

Model	Generator Level			
	ACC	Precision	Recall	F1
ResNet [51]	99.67	99.67	99.67	99.67
Xception [26]	99.84	99.84	99.84	99.84
ViT [53]	98.73	98.73	98.73	98.73
CViT [24]	99.93	99.93	99.93	99.93
CEViT [25]	99.94	99.94	99.94	99.94
Ours	99.95	99.98	99.97	99.97

baselines. Next, we plan to design a lightweight detector to jointly dig hierarchical clues.

Effects of appearance-edge cross-attention. We further studied the importance of AECA through cross-generator evaluation. In Table XIII, we noticed that a nearly 1.4% increase of AUC could be achieved by introducing AECA. It turns out that the diverse global fusion between multi-grained appearance and edge domains is helpful for detecting comprehensive counterfeit traces.

Facial image frequency analysis. We visualized the average spectrum of authentic and manipulated images from various generators. We utilized the Fourier transform to examine artifacts produced by generative networks. We randomly selected 5,000 images for Fourier transform, and averaged the results for spectral analysis. The result is illustrated in Fig. 7. We observed that authentic faces from CelebAHQ, as well as fake faces generated by diffusion-based techniques, contain few artifacts. It is noticed that the face synthesized by the diffusion-based model is closer to the authentic face than GAN-based methods. Consequently, diffusion-based generators pose a greater threat to deepfake detection.

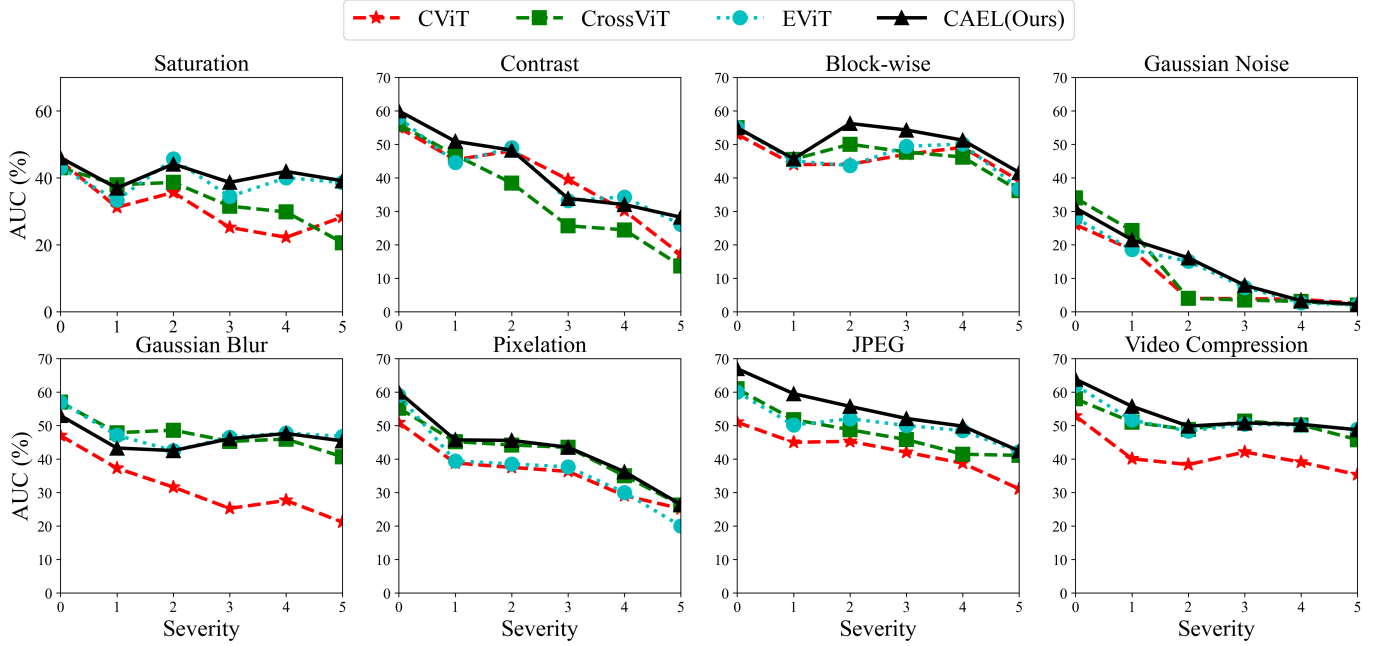


Fig. 8: Robustness to unseen image distortions.

TABLE XIII: The ablation of the AECA module.

Training Set	Model	Testing Set	
		GAN-syn.	
		ACC	AUC
Diffusion-syn.	ours w/o AECA	50.47	91.35
	ours w/ AECA	50.60	92.73

TABLE XIV: The effect of the depth of the edge transformer encoder and the number of multi-grained appearance-edge transformer blocks.

Training Set	Model	Testing Set			
		GAN-syn.			
		ACC	AUC	Params(M)	Flops(G)
Diffusion-syn.	E=0	50.12	87.33	130.27	2.05
	E=1	50.24	90.89	139.73	2.07
	E=2	50.49	91.78	149.18	2.09
	E=3	50.60	92.73	158.63	2.11
	E=4	50.51	92.04	168.09	2.13
	K=1	50.09	86.75	92.14	1.99
	K=2	50.11	88.20	114.31	2.03
	K=3	50.44	90.65	136.47	2.07
	K=4	50.60	92.73	158.63	2.11
	K=5	50.57	92.56	180.80	2.15

Depth of edge transformer encoder and the number of multi-grained appearance-edge transformer blocks. We inspected the effect of the depth of the edge transformer encoder. As shown in Table XIV, we observed that the performance of CAEL gradually grows with the increase of

TABLE XV: The ablation of various fusions of different architectures.

Model	Fusion	ACC	AUC
F+E	Concatenation	50.15	86.61
	Summation	50.26	87.72
	Cross-Attention	50.37	88.86
C+E	Concatenation	50.29	88.17
	Summation	50.37	89.21
	Cross-Attention	50.45	90.32
F+C+E	Concatenation	50.48	90.95
	Summation	50.54	91.56
	Cross-Attention	50.60	92.73

edge transformer blocks. The AUC achieves the maximum when three blocks are involved. We also observed the impacts of the number of the MAET on detection performance by varying the depth K , and other parameters remain unchanged. Using more than four transformer blocks in MAET increases FLOPs and parameters without any improvement in accuracy. We suspected that too many blocks would lead to information redundancy, thus reducing the representation ability.

Robustness analysis. We aimed to evaluate the robustness of detectors against diverse unseen image distortions by training them on GenFace, and testing their performance on FF++ [57]. We tested models on different image corruptions with a series of intensity levels, including saturation adjustments, contrast modifications, block-wise distortions, white Gaussian noise addition, blurring, pixelation, and video compression using the H.264 codec. When applying corruptions of varying intensities, the changes of AUC for all techniques are shown in Fig. 8.

The statistics show that our model consistently outperforms all other methods for all types of image corruption.

Comparison of different fusion schemes. We further investigated the impact of various fusion schemes. Table XV shows the performance of various fusion strategies for different models. Among all the compared schemes, the proposed cross-attention strategies achieve the best AUC, showing the effectiveness of the diverse global fusion between appearance and edge features.

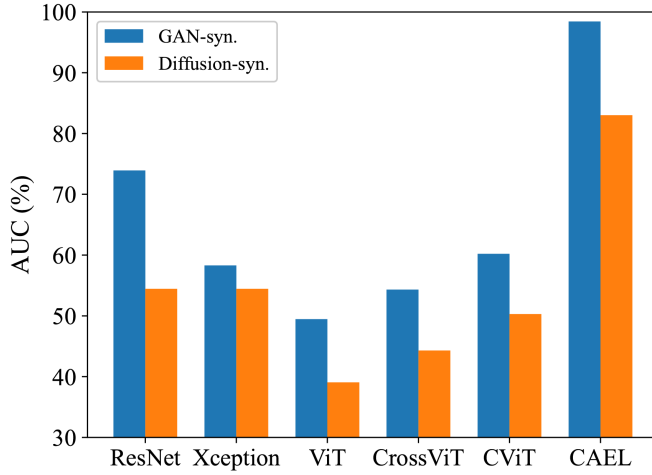


Fig. 9: Comparison of the performance of the model on diffusion-based and GAN-based generators.

VI. CONCLUSION

In this paper, we establish a large-scale, diverse, and fine-grained high-fidelity deepfake dataset, namely GenFace, along with a robust deepfake detector. Our GenFace dataset contains novel forgery methods such as the diffusion-based generator, achieving diversity, high image quality, and hierarchical fine-grained classification, which benefits developing more robust deepfake detection techniques. Moreover, we propose the cross appearance-edge learning model to capture rich multi-grained appearance and edge global fusion forgery traces. In the future, we intend to introduce diverse facial images manipulated by advanced generators for fine-grained partitioning, to enrich data volume and diversity.

REFERENCES

- [1] X. Yang, Y. Li, and S. Lyu, "Exposing deep fakes using inconsistent head poses," in *2019 - 2019 IEEE International Conference on Acoustics, Speech and Signal Processing (ICASSP)*, 2019, pp. 8261–8265.
- [2] R. Wang, F. Juefei-Xu, L. Ma, X. Xie, Y. Huang, J. Wang, and Y. Liu, "Fakespotter: A simple yet robust baseline for spotting ai-synthesized fake faces," in *Proceedings of the Twenty-Ninth International Joint Conference on Artificial Intelligence (IJCAI)*, ser. IJCAI'20, 2021.
- [3] A. Rössler, F. Cozzolino, L. Verdoliva, C. Riess, J. Thies, and M. Niessner, "Faceforensics++: Learning to detect manipulated facial images," in *2019 IEEE/CVF International Conference on Computer Vision (ICCV)*, 2019, pp. 1–11.
- [4] Y. Li, X. Yang, P. Sun, H. Qi, and S. Lyu, "Celeb-df: A large-scale challenging dataset for deepfake forensics," in *2020 IEEE/CVF Conference on Computer Vision and Pattern Recognition (CVPR)*, June 2020, pp. 3204–3213.
- [5] B. Dolhansky, J. Bitton, B. Pflaum, J. Lu, R. Howes, M. Wang, and C. Canton-Ferrer, "The deepfake detection challenge dataset," *ArXiv*, vol. abs/2006.07397, 2020.
- [6] L. Jiang, R. Li, W. Wu, C. Qian, and C. C. Loy, "Deeperforensics-1.0: A large-scale dataset for real-world face forgery detection," in *2020 IEEE/CVF Conference on Computer Vision and Pattern Recognition (CVPR)*, June 2020, pp. 2886–2895.
- [7] H. Dang, F. Liu, J. Stehouwer, X. Liu, and A. K. Jain, "On the detection of digital face manipulation," in *2020 IEEE/CVF Conference on Computer Vision and Pattern Recognition (CVPR)*, 2020, pp. 5780–5789.
- [8] Y. He, B. Gan, S. Chen, Y. Zhou, G. Yin, L. Song, L. Sheng, J. Shao, and Z. Liu, "ForgeryNet: A versatile benchmark for comprehensive forgery analysis," in *2021 IEEE/CVF Conference on Computer Vision and Pattern Recognition (CVPR)*, 2021, pp. 4358–4367.
- [9] X. Hou, K. Sun, L. Shen, and G. Qiu, "Improving variational autoencoder with deep feature consistent and generative adversarial training," *Neurocomputing*, vol. 341, pp. 183–194, 2019. [Online]. Available: <https://www.sciencedirect.com/science/article/pii/S0925231219303157>
- [10] I. Goodfellow, J. Pouget-Abadie, M. Mirza, B. Xu, D. Warde-Farley, S. Ozair, A. Courville, and Y. Bengio, "Generative adversarial nets," in *Advances in Neural Information Processing Systems (NIPS)*, 2014, pp. 2672–2680.
- [11] H. Li, X. Hou, Z. Huang, and L. Shen, "Stylegene: Crossover and mutation of region-level facial genes for kinship face synthesis," in *2023 IEEE/CVF Conference on Computer Vision and Pattern Recognition (CVPR)*, 2023, pp. 20960–20969.
- [12] T. Karras, M. Aittala, S. Laine, E. Härkönen, J. Hellsten, J. Lehtinen, and T. Aila, "Alias-free generative adversarial networks," in *Neural Information Processing Systems (NIPS)*, 2021. [Online]. Available: <https://api.semanticscholar.org/CorpusID:235606261>
- [13] T. Karras, S. Laine, M. Aittala, J. Hellsten, J. Lehtinen, and T. Aila, "Analyzing and improving the image quality of stylegan," in *2020 IEEE/CVF Conference on Computer Vision and Pattern Recognition (CVPR)*, 2020, pp. 8107–8116.
- [14] J. Ho, A. Jain, and P. Abbeel, "Denoising diffusion probabilistic models," *ArXiv*, vol. abs/2006.11239, 2020. [Online]. Available: <https://api.semanticscholar.org/CorpusID:219955663>
- [15] A. Croft, "From porn to scams, deepfakes are becoming a big racket and that's unnerving business leaders and lawmakers," <https://fortune.com/2019/10/07/porn-to-scams-deepfakes-big-racket-unnerving-business-leaders-and-lawmakers/>, 2020, accessed: 2020-10-03.
- [16] U. C. London, "Deepfakes' ranked as most serious AI crime threat," <https://www.sciencedaily.com/releases/2020/08/20200804085908.htm>, 2021, accessed: 2021-05-01.
- [17] X. Yao, A. Newson, Y. Gousseau, and P. Hellier, "A latent transformer for disentangled face editing in images and videos," in *2021 IEEE/CVF International Conference on Computer Vision (ICCV)*, 2021, pp. 13 769–13 778.
- [18] W. Huang, S. Tu, and L. Xu, "Ia-faces: A bidirectional method for semantic face editing," *Neural Networks*, vol. 158, pp. 272–292, 2023. [Online]. Available: <https://www.sciencedirect.com/science/article/pii/S0893608022004579>
- [19] M. Pernuš, V. Štruc, and S. Dobrišek, "Maskfacegan: High resolution face editing with masked gan latent code optimization," *IEEE Transactions on Image Processing (TIP)*, 2023.
- [20] Q. Li, W. Wang, C. Xu, and Z. Sun, "Learning disentangled representation for one-shot progressive face swapping," *arXiv preprint arXiv:2203.12985*, 2022.
- [21] Y. Xu, B. Deng, J. Wang, Y. Jing, J. Pan, and S. He, "High-resolution face swapping via latent semantics disentanglement," in *2022 IEEE/CVF Conference on Computer Vision and Pattern Recognition (CVPR)*, 2022, pp. 7632–7641.
- [22] T. Karras, S. Laine, and T. Aila, "A style-based generator architecture for generative adversarial networks," in *2019 IEEE/CVF Conference on Computer Vision and Pattern Recognition (CVPR)*, 2019, pp. 4396–4405.
- [23] X. Guo, X. Liu, Z. Ren, S. Grosz, I. Masi, and X. Liu, "Hierarchical fine-grained image forgery detection and localization," in *2023 IEEE/CVF Conference on Computer Vision and Pattern Recognition (CVPR)*, 2023, pp. 3155–3165.
- [24] D. Wodajo and S. Atanfu, "Deepfake video detection using convolutional vision transformer," 2021, arXiv preprint arXiv:2102.11126.
- [25] D. A. Cocomini, N. Messina, C. Gennaro, and F. Falchi, "Combining efficientnet and vision transformers for video deepfake detection," in

- International Conference on Image Analysis and Processing (ICIAP)*. Springer, 2022, pp. 219–229.
- [26] F. Chollet, “Xception: Deep learning with depthwise separable convolutions,” in *Proceedings of the IEEE Conference on Computer Vision and Pattern Recognition (CVPR)*, 2017, pp. 1800–1807.
- [27] C. Si, W. Yu, P. Zhou, Y. Zhou, X. Wang, and S. Yan, “Inception transformer,” in *Advances in Neural Information Processing Systems (NIPS)*, S. Koyejo, S. Mohamed, A. Agarwal, D. Belgrave, K. Cho, and A. Oh, Eds., vol. 35. Curran Associates, Inc., 2022, pp. 23 495–23 509. [Online]. Available: https://proceedings.neurips.cc/paper_files/paper/2022/file/94e85561a342de88b559b72c9b29f638-Paper-Conference.pdf
- [28] N. Kanopoulos, N. Vasanthavada, and R. L. Baker, “Design of an image edge detection filter using the sobel operator,” *IEEE Journal of Solid-state Circuits*, vol. 23, no. 2, pp. 358–367, 1988.
- [29] J. Canny, “A computational approach to edge detection,” *IEEE Transactions on Pattern Analysis and Machine Intelligence*, no. 6, pp. 679–698, 1986.
- [30] G. E. Sotak Jr and K. L. Boyer, “The laplacian-of-gaussian kernel: a formal analysis and design procedure for fast, accurate convolution and full-frame output,” *Computer Vision, Graphics, and Image Processing*, vol. 48, no. 2, pp. 147–189, 1989.
- [31] D. Marr and E. Hildreth, “Theory of edge detection,” *Proceedings of the Royal Society of London. Series B. Biological Sciences*, vol. 207, no. 1167, pp. 187–217, 1980.
- [32] N. Ahmed, T. Natarajan, and K. Rao, “Discrete cosine transform,” *IEEE Transactions on Computers*, vol. C-23, no. 1, pp. 90–93, 1974.
- [33] J. Wang, Z. Wu, W. Ouyang, X. Han, J. Chen, Y.-G. Jiang, and S.-N. Li, “M2tr: Multi-modal multi-scale transformers for deepfake detection,” in *Proceedings of the 2022 International Conference on Multimedia Retrieval (ICMR)*, ser. ICMR ’22. New York, NY, USA: Association for Computing Machinery, 2022, p. 615–623. [Online]. Available: <https://doi.org/10.1145/3512527.3531415>
- [34] T. Karras, T. Aila, S. Laine, and J. Lehtinen, “Progressive growing of GANs for improved quality, stability, and variation,” in *International Conference on Learning Representations (ICLR)*, 2018. [Online]. Available: <https://openreview.net/forum?id=Hk99zCeAb>
- [35] A. Rössler, D. Cozzolino, L. Verdoliva, C. Riess, J. Thies, and M. Nießner, “Faceforensics: A large-scale video dataset for forgery detection in human faces,” *CoRR*, vol. abs/1803.09179, 2018. [Online]. Available: <http://arxiv.org/abs/1803.09179>
- [36] J. Thies, M. Zollhöfer, M. Stamminger, C. Theobalt, and M. Nießner, “Face2face: Real-time face capture and reenactment of rgb videos,” in *Proceedings of the IEEE Conference on Computer Vision and Pattern Recognition (CVPR)*, June 2016, pp. 2387–2395.
- [37] A. Rössler, D. Cozzolino, L. Verdoliva, C. Riess, J. Thies, and M. Nießner, “Faceforensics++: Learning to detect manipulated facial images,” in *Proceedings of the IEEE International Conference on Computer Vision (ICCV)*, 2019, pp. 1–11.
- [38] “Deepfake,” <https://github.com/deepfakes/>, 2020, accessed: 2020-09-03.
- [39] FaceSwap, “Faceswap,” <https://github.com/MarekKowalski/FaceSwap>, 2020, accessed: 2020-09-03.
- [40] R. Rombach, A. Blattmann, D. Lorenz, P. Esser, and B. Ommer, “High-resolution image synthesis with latent diffusion models,” in *Proceedings of the IEEE/CVF conference on computer vision and pattern recognition*, 2022, pp. 10 684–10 695.
- [41] Z. Huang, K. C. Chan, Y. Jiang, and Z. Liu, “Collaborative diffusion for multi-modal face generation and editing,” in *Proceedings of the IEEE/CVF Conference on Computer Vision and Pattern Recognition*, 2023, pp. 6080–6090.
- [42] K. Preechakul, N. Chatthee, S. Wizadwongsa, and S. Suwajanakorn, “Diffusion autoencoders: Toward a meaningful and decodable representation,” in *IEEE Conference on Computer Vision and Pattern Recognition (CVPR)*, 2022.
- [43] K. Kim, Y. Kim, S. Cho, J. Seo, J. Nam, K. Lee, S. Kim, and K. Lee, “Diffface: Diffusion-based face swapping with facial guidance,” *arXiv preprint arXiv:2212.13344*, 2022.
- [44] Y. Wang, K. Yu, C. Chen, X. Hu, and S. Peng, “Dynamic graph learning with content-guided spatial-frequency relation reasoning for deepfake detection,” in *Proceedings of the IEEE/CVF Conference on Computer Vision and Pattern Recognition*, 2023, pp. 7278–7287.
- [45] Z. Liu, X. Qi, and P. H. Torr, “Global texture enhancement for fake face detection in the wild,” in *Proceedings of the IEEE/CVF conference on computer vision and pattern recognition*, 2020, pp. 8060–8069.
- [46] Z. Wang, J. Bao, W. Zhou, W. Wang, H. Hu, H. Chen, and H. Li, “Dire for diffusion-generated image detection,” in *2023 IEEE/CVF International Conference on Computer Vision (ICCV)*, 2023, pp. 22 388–22 398.
- [47] U. Ojha, Y. Li, and Y. J. Lee, “Towards universal fake image detectors that generalize across generative models,” in *Proceedings of the IEEE/CVF Conference on Computer Vision and Pattern Recognition*, 2023, pp. 24 480–24 489.
- [48] Z. Liu, P. Luo, X. Wang, and X. Tang, “Deep learning face attributes in the wild,” in *2015 IEEE International Conference on Computer Vision (ICCV)*, 2015, pp. 3730–3738.
- [49] T. Karras, S. Laine, and T. Aila, “A style-based generator architecture for generative adversarial networks,” *IEEE Transactions on Pattern Analysis and Machine Intelligence*, vol. 43, no. 12, pp. 4217–4228, 2021.
- [50] C.-F. R. Chen, Q. Fan, and R. Panda, “Crossvit: Cross-attention multi-scale vision transformer for image classification,” in *Proceedings of the IEEE International Conference on Computer Vision (CVPR)*, October 2021, pp. 357–366.
- [51] K. He, X. Zhang, S. Ren, and J. Sun, “Deep residual learning for image recognition,” in *Proceedings of the IEEE Conference on Computer Vision and Pattern Recognition (CVPR)*, 2016, pp. 770–778.
- [52] K. Simonyan and A. Zisserman, “Very deep convolutional networks for large-scale image recognition,” in *International Conference on Learning Representations (ICLR)*, 2015.
- [53] A. Dosovitskiy, L. Beyer, A. Kolesnikov, D. Weissenborn, X. Zhai, T. Unterthiner, M. Dehghani, M. Minderer, G. Heigold, S. Gelly, J. Uszkoreit, and N. Houlsby, “An image is worth 16x16 words: Transformers for image recognition at scale,” in *International Conference on Learning Representations (ICLR)*, Austria, 2021.
- [54] Y. Luo, Y. Zhang, J. Yan, and W. Liu, “Generalizing face forgery detection with high-frequency features,” in *Proceedings of the IEEE/CVF conference on computer vision and pattern recognition*, 2021, pp. 16 317–16 326.
- [55] A. Buslaev, V. I. Iglovikov, E. Khvedchenya, A. Parinov, M. Druzhinin, and A. A. Kalinin, “Albumentations: Fast and flexible image augmentations,” *Information*, vol. 11, no. 2, 2020.
- [56] D. P. Kingma and J. Ba, “Adam: A method for stochastic optimization,” in *International Conference on Learning Representations (ICLR)*, San Diego, CA, USA, Conference Track Proceedings, May 2015.
- [57] L. Jiang, R. Li, W. Wu, C. Qian, and C. C. Loy, “Deeperforensics-1.0: A large-scale dataset for real-world face forgery detection,” in *Proceedings of the IEEE Conference on Computer Vision and Pattern Recognition (CVPR)*, June 2020, pp. 2886–2895.